Computational mechanistic studies on persulfate assisted p-phenylenediamine polymerization

Yusif Abdullayev*[a,b], Ramil Rzayev[a,c], and Jochen Autschbach[d]

[a] Department of Chemical Engineering, Baku Engineering University, Hasan Aliyev str. 120, Baku, Absheron, AZ0101, Azerbaijan. Email: yabdullayev@beu.edu.az

[b] Institute of Petrochemical Processes, Azerbaijan National Academy of Sciences, Khojaly ave. 30, Az1025, Baku, Azerbaijan

[c] Institute of Polymer Materials, Azerbaijan National Academy of Sciences, AZ5004, S. Vurgun Str., 124, Sumgait, Azerbaijan

[d] Department of Chemistry, University at Buffalo, State University of New York, Buffalo, New York 14260-3000, United States.

Abstract: p-phenylenediamine (p-PDA) is a monomer of many important polymers such as kevlar, twaron, poly-p-PDA. Most of the noticed polymers formation is initiated by a free-radical, but their polymerization mechanism is not elucidated computationally. The proposed study helps to fully understand the frequently utilized initiator/oxidant, potassium persulfate ($K_2S_2O_8$) role in the aromatic diamines polymerization, which support experimental protocols, and a polymer scope. The formation of the poly-p-PDA is studied with the density functional theory (DFT) B3LYP-D3 functional using experimental polymerization parameters (0^{o}C and aqueous media). $K_2S_2O_8$ initiated free-radical polymerization of p-PDA is studied in detail, taking into account sulfate free-radical $(SO_4^-)^{\cdot}$, SFR, persulfate anion $(S_2O_8)^{2-}$, PA and $K_2S_2O_8$ cluster, PP. The reaction mechanism is calculated as the conversion of p-PDA to free-radical, the p-PDA free-radical attack to the next p-PDA (dimerization), ammonia extrusion from the dimer adduct, the dimer adduct conversion to the free-radical (completion of p-PDA polymerization cycle) for the polymer chain elongation. Calculations show that the dimerization step is the rate-limiting step with a 29.2 kcal/mol energy barrier when SFR initiates polymerization. In contrast, the PA-assisted dimerization energy barrier is only 12.7 kcal/mol. PP supported polymerization is calculated to have very shallow energy barriers completing the polymerization cycle, i.e., dimerization (**TS2K**, $\Delta G^{\ddagger}$=11.6 kcal/mol) and ammonia extrusion (**TS3K**, $\Delta G^{\ddagger}$=6.7 kcal/mol).

Keywords: Potassium persulfate, polymerization, p-phenylenediamine, noncovalent interaction, DFT, transition state, energy barrier.

1. Introduction

Phenylenediamine (PPD) based polymers are very vital in the industry because of the wide range of applications: conductive material in energy storage devices [1], impedimetric sensor for pentoses [2], photocatalysis [3], biomedical devices [4], corrosion protection [3], and heavy metal absorbents [5,6]. Because of the promising thermal stability and high antioxidant properties, such as against 2,2-diphenyl-1-picrylhydrazyl free-radical and hydrogen peroxide poly-PPD polymers were suggested utilizing in optoelectronic devices [7]. Poly-PPD was exploited as a material for thin-film electroluminescent devices owing to π bond in the backbone that results in excellent emission intensity [8]. Poly-ortho-PPD was oxidized by potassium bichromate to form submicrometer-scale colloid, which exploited to absorb and quench dye-labeled single-stranded DNA efficiently [9].

Because of the aforementioned strategic applications, extensive research has been carried out to synthesize and characterize poly-PPDs [10]. The electrochemical synthesis of poly-o-PPD in an aqueous medium was improved by adjusting the switching potential to enhance the growth of the polymer [11]. Ammonium persulfate assisted synthesis of poly-m-PPD, the role of pH value on the polymer growth, and morphology of formed nanostructure were studied [9]. A facile synthesis protocol of poly-o-PPD was proposed, and the polymer was utilized in submicrosphere-supported gold nanoparticle formation. The existence of amino groups and π bonds in poly-o-PPD stabilizes gold nanoparticles that render selective oxidation of benzyl alcohol [12].

Identification of a polymerization reaction mechanism can contribute to controlling and directing a reaction toward the desired product formation. Since the importance of polymeric materials, polymerization reactions have become a subject of computational research long ago [13]. Xanthates polymerization reaction mechanism and HOMO-LUMO energy were calculated up to hexamer level [14]. Free radical polymerization reaction rate was studied with density functional theory (DFT) [15]. Conjugated polymers orbital energies were calculated and correlated with experimental results. It was identified that at the trimer level, orbital energies well correlated with experimental results [16]. An extensive theoretical analysis of the free-radical copolymerization of maleic anhydride with α-olefins was performed by DFT [17]. The copolymerization reaction mechanism between cyclic ketene acetals and traditional vinyl monomers was studied with DFT [18]. Radical mediated cyclization [3+2] based allyl

radical polymerization reaction mechanism was studied with DFT [19]. The Cu–arylacetylide polymerization reaction mechanism was investigated theoretically [20]. The phenylenediamine polymerization mechanism attracted scientists decades ago: Lakard et al. investigated the p-PDA polymerization mechanisms with voltammetry and ab initio studies. The mechanism was suggested in the computational research without a saddle point allocation. Only hypothesized structures were optimized. The formation energies of all the species were determined and used in the mechanism elucidation, which needs to be improved with a new approach [21].

Poly(o-phenylenediamine) oligomer structures were studied with DFT and TD-DFT calculations. Experimental and theoretical UV-vis and IR spectra of the various conformers of poly(o-phenylenediamine) were correlated [22]. Despite the previous efforts, the p-PDA polymerization mechanism with the support of antioxidants like sodium persulfate is still intriguing and requires computational consideration. So, we computationally investigated persulfate mediated polymerization of p-PDA taking into account the model reaction of Scheme 1. The $K_2S_2O_8$ assisted p-PDA polymerization reaction is considered in the proposed computational study because, in most of the experimental studies, [23-26] persulfate precursors are taken as oxidants (Scheme 1).

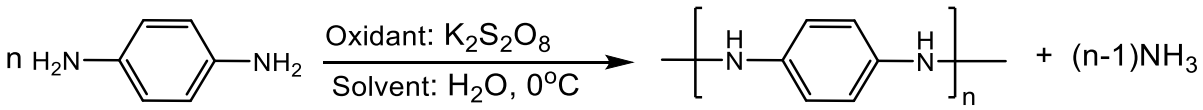

Scheme 1: p-PDA polymerization reaction considered in the quantum chemical calculations.

2. Computational Details

The Gaussian 16 package was utilized for all calculations [27]. The computations were performed by using DFT/B3LYP functional [28,29] with Grimme's empirical dispersion correction (D3) [30]. 6-31G*[31] basis sets were used for H, C, N, and O atoms. For S and K atoms, the 6-31++G(d,p) basis was exploited according to recent recommendations [32]. The PP route structures were reoptimized with M062-X functional, and comparative RPs were designed along with B3LYP-D3 results. Calculations show that B3LYP-D3 is better for describing the p-PDA polymerization mechanism, particularly for the ammonia extrusion step (See SI, Figure S4). The reaction was calculated based on the experimental reaction conditions (1atm, 273.15 K). Solvent effects were included via a self-consistent reaction field (SCRF) continuum solvation model with a dielectric constant for water because it was used experimentally. An intrinsic reaction coordinate (IRC) search was executed to confirm the obtained transition states (one imaginary frequency) connected to intermediates (zero imaginary frequency) structures. All the intermediate and transition state

structures were calculated without geometry constraints. Optimized Cartesian coordinates, total energies, Gibbs energies, and enthalpies of all structures are provided in supporting information (SI). The SFR route (green) structures were optimized according to the free-radical mode (charge: -1, multiplicity: 2). In the case of sulfate dimer (PA route), the anion mode (charge: -2, multiplicity: 1) was exploited for all species (Figure 1). The PP route structures were optimized in neutral mode (charge: 0, multiplicity: 1) since the neutral PP cluster was used to initiate the p-PDA polymerization.

3. Results and Discussion

The conversion of p-PDA into free-radical is required to initiate the polymerization reaction. Experimentally it was carried out by mixing the monomer and $K_2S_2O_8$ in aqueous media [24,33]. So, we initially decided to consider the possible interaction of water molecules on the persulfate precursor. We start the computation to observe the mutual role of $S_2O_8^{2-}$ and water on the p-PDA transition to free-radical. Therefore, the free-radical formation step of p-PDA was simulated with $S_2O_8^{2-}$+2H_2O (**TS+2H$_2$O**) and $S_2O_8^{2-}$+H_2O (**TS+H$_2$O**) clusters to show the energy barriers. Two water molecules are incorporated into $S_2O_8^{2-}$; one is taking part in direct deprotonation of the p-PDA amine group (See SI, Figure S1), and the second water molecule links two sulfate ions of $S_2O_8^{2-}$ via noncovalent interaction (NCI) (H3-O3: 2.17 Å, H4-O4: 1.90 Å) in **TS+2H$_2$O** structure which requires 58.8 kcal/mol to detach proton from the p-PDA amine group. The second transition state (TS) structure, **TS+H$_2$O**, requires 6.7 kcal less energy than **TS+2H$_2$O** to remove proton from the p-PDA amine group. The result shows that additional water

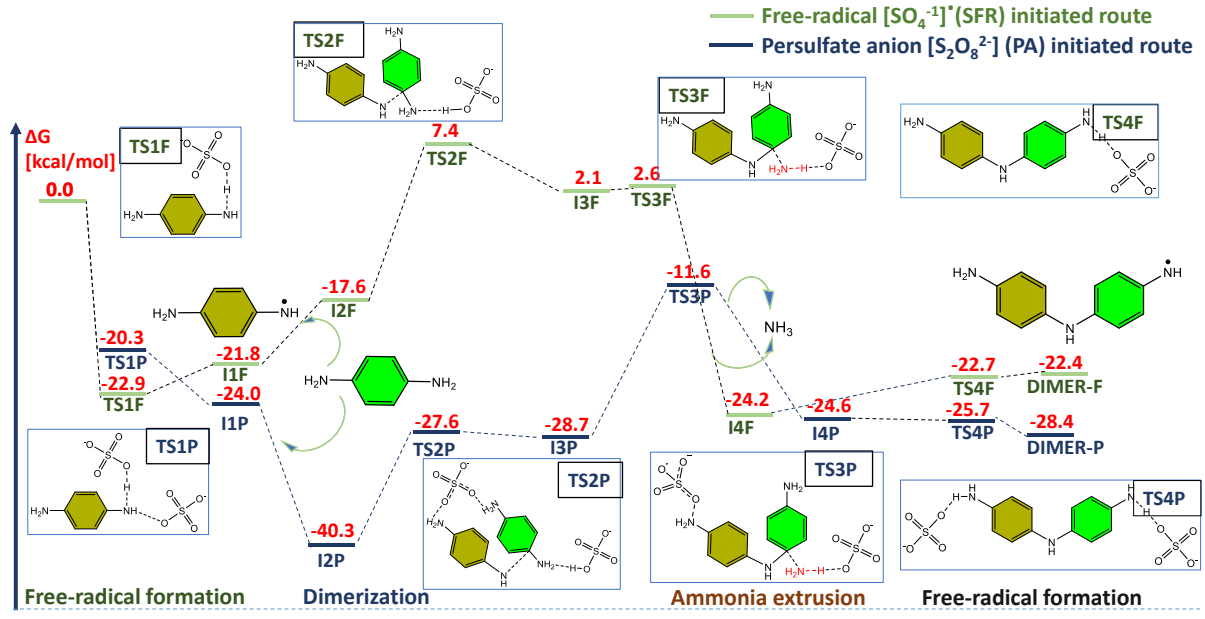

Figure 1. Reaction profile for p-PDA dimerization: SFR initated route (blue), PA initated route (green).

incorporation does not facilitate free-radical formation (See SI for detailed discussion).

Alternatively, a TS for the persulfate sulfur atom direct incorporation for the p-PDA conversion to free-radical via removing the p-PDA amine group proton was successfully located (See SI, Figure S2). A similar high energy barrier was obtained for (**TS-S**) 51.7 kcal/mol, which directed us to focus on the SFR, PA, and PP routes. Because of the previous suggestion [27] about possible decomposition probabilities of persulfate ion in aqueous media, the p-PDA dimerization is calculated trice with SFR, PA, and PP.

SFR route: Considering the decomposition probability of sulfate dimer (persulfate) into two SFR the dimerization cycle of p-PDA was first calculated with SFR (Figure 1, blue route). As seen from the reaction profile (RP), the energy of the pre-reaction complex is not described before **TS1F** since p-PDA conversion to free-radical is a barrierless process (See SI, Table S1). The free-radical attack on the second monomer is calculated to have the highest barrier (29.2 kcal/mol). The optimized structure of **TS2F** shows that (See SI, Figure S3) protonated SFR is only making a hydrogen bond with the monomer amine group via 1.664 Å distance (N2-H1). The distance of the free-radical nitrogen atom (N1) attack to the monomer carbon atom (C) is calculated to be 1.864 Å. Then ammonia extrusion step (**TS3F**, See SI, Figure S5 for optimized structure) is observed to be barrierless (0.4 kcal/mol) to get **I4F** (p-PDA dimer). For further elongation of the polymer chain, **I4F** conversion to free-radical is required, which is again a barrierless process (-0.3 kcal/mol) as initially observed (**TS1F**) in **I1F** formation.

PA route: The PA assisted conversion of p-PDA (**TS1P**) to free-radical is observed to be barrierless like the SFR route (See SI, Table S2). The addition of p-PDA monomer to the p-PDA free-radical is going through a lower energy barrier (**TS2P**, 12.7 kcal/mol) compared to the SFR promoted dimerization (**TS2F**) barrier. This fact can be explained by the existence of the additional sulfate ion in **TS2P** structure. Sulfate ion binds p-PDA monomer and free-radical via hydrogen bonding between the amine group hydrogens (H2, H3) and sulfate oxygen atoms (O2, O3) and facilitates the attack of the free-radical to the next p-PDA carbon atom in the aromatic ring (See SI, Figure S3). The second sulfate ion is acting similar to what we noticed in **TS2F** structure: Hydrogen (H1) of the protonated sulfate forms a hydrogen bond with amine (N2) group to elongate C-N2 (1.427 Å) bond to ease dimerization. Conversely, the ammonia extrusion step is calculated to be higher in energy (**TS3P**, 17.1 kcal/mol) than the same step at SFR (**TS3F**, no energy barrier). It can be scrutinized with a lower electron density of free-radical because of the sulfate interaction with the p-PDA primary amine side. The transition of **I4P** to free-radical (**DIMER-P**) is calculated to go without an energy barrier as initially observed in the SFR route.

PP route: PP cluster effect on the dimerization of p-PDA is calculated to see the integrated effect (including potassium) of PP salt on TSs (Figure 2). As seen in RPs of Figure 1, the free-radical formation step is without an energy barrier, which is observed for the PP route as well (the energy of the pre-reaction complex is omitted. See SI, Table S3). The next TSs and intermediate structures lowest

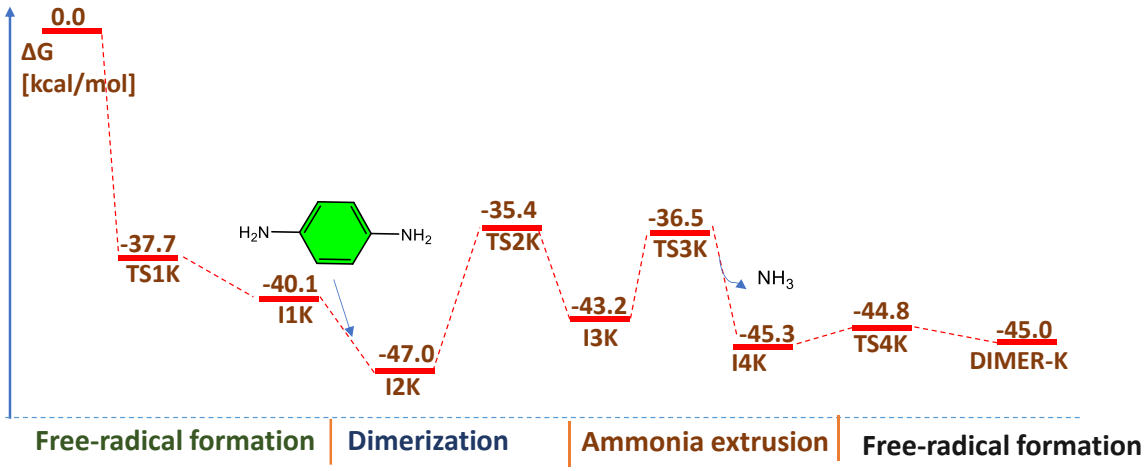

Figure 2. Reaction profile for p-PDA dimerization via PP salt.

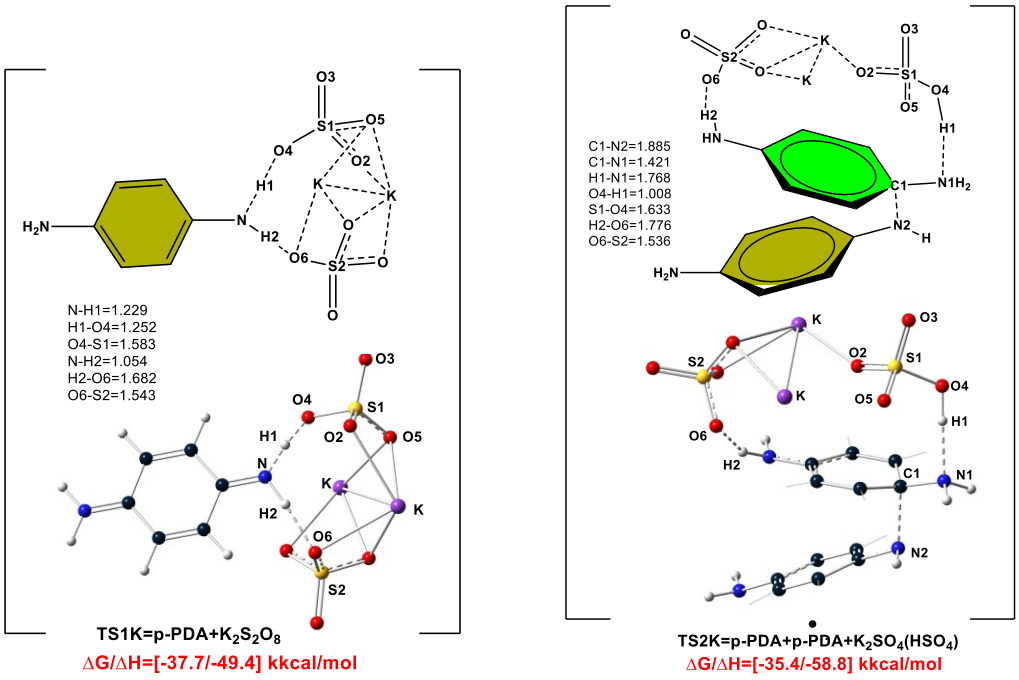

Figure 3. Optimized structures of **TS1K** and **TS2K** TSs with important bond lengths (given in Å). Hydrogen atoms are omitted for the sake of clarity.

formation energies and energy barriers implies to accept the PP route as the favorable thermodynamic path for the p-PDA polymerization. The free-radical formation TS (**TS1K**, $\Delta G^{\ddagger}$=-37.7) is calculated to have the lowest energy compared to the SRF and PA routes. Optimized structure of **TS1K** shows the p-PDA amine group penetration (like a 'key-lock' analogy) to PP cluster renders to hold the structure for easy proton transition (N-H1; 1.229 Å and H1-O4; 1.252 Å) to PP (Figure 3) through NCI (H2-O6; 1.682 Å). Two potassium atoms in the middle of PP bind sulfates to boost the oxidant abilities. Further analysis of the next TS (**TS2K**, $\Delta G^{\ddagger}$=-35.4) structure confirms NCI's role in the dimerization step. Compared to the analogous TS (**TS2F**), dual binding (H2-O6; 1.776 and N1-H1; 1.768) of PP via amine groups (at the para position) to p-PDA structure (**TS2K**) considerably facilitates the free-radical attack through 11.6 kcal/mol energy barrier (Figure 3).

The ammonia extrusion step (**TS3K)** is calculated to be 6.7 kcal/mol higher in energy, which is 10.4 kcal lower than the corresponding TS (**TS3P**) in the PA route. The NCI (hydrogen bonding: H2-O6; 1.669 Å) role is to keep the PP cluster on the top of p-PDA to ease ammonia pup-up via C1-N1; 1.996 Å bond length. Ammonia was detected during the PP initiated p-PDA polymerization in the previous experimental study, which is in good agreement with our calculation regarding the ammonia extrusion step [25]. The proton transfer from the PP cluster to the p-PDA NH_2 group is straightforward via O4-H1-N1; 1.761, 1.041 Å distances (Figure 4). Conversion of p-PDA dimer to free-radical (**TS4K**) is calculated to have 7.1 kcal lower formation Gibbs energy than the monomer conversion to free-radical (**TS1K**). It can be explained with the addition of the second aromatic ring, which increases electron density in the amine group: Calculated Mulliken charge analysis shows that the charge of amine group N atom in **TS1K**

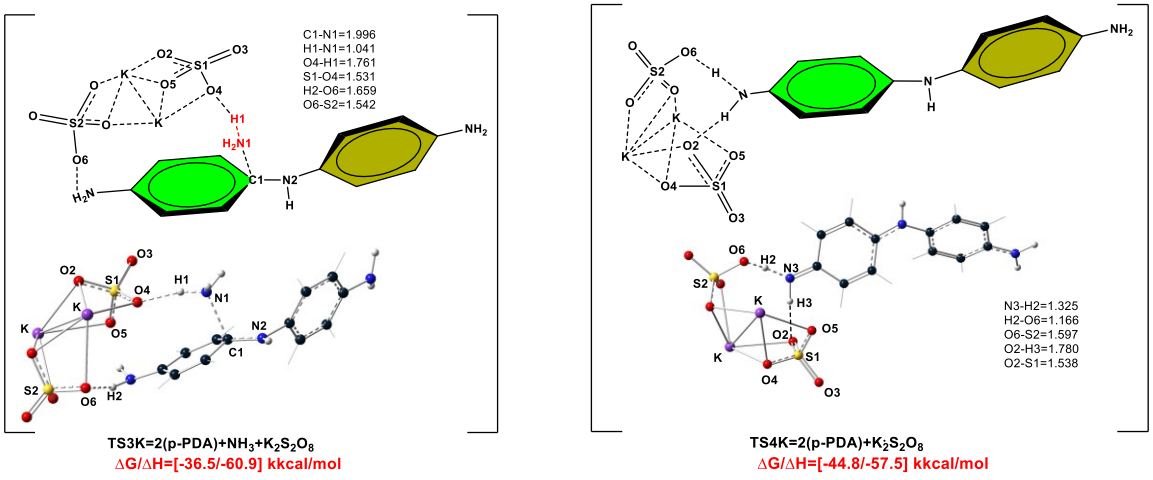

Figure 4. Optimized structures of **TS3K** and **TS4K** TSs with important bond lengths (given in Å). Hydrogen atoms are omitted for the sake of clarity.

subjected to proton transfer is -0.72, whereas the same nitrogen (N3) charge in **TS4K** is -0.81, which renders proton transfer via a little longer bond length (N3-H2; 1.325 Å). The same bond (N-H1) at the optimized **TS1K** structure is 1.229 Å. Based on the bond lengths and charges mentioned above, we can propose that free-radical is more likely to form relative to the monomer (p-PDA, **TS1K**) in a long chain of poly-PDA.

Hypothesized mechanisms in the previous experimental studies proposed p-PDA conversion to free-radical not only on p-PDA head (amine group) but also via proton migration the formation of side radicals was suggested. Observations showed that head-to-head (amine groups) polymerization is more common than ring-to-ring (phenyl groups links) or head-to-ring polymerization [23,25].

We tried to calculate the $\dot{N}H - C_6H_4 - NH_2 \overset{\sim H}{\longrightarrow} NH_2 - \dot{C}_6H_3 - NH_2$ rearrangement to shed light to p-PDA polymerization styles. Figure 5 describes proton migration according to the route mentioned above. The phenyl ring proton is elongated up to 1.55 Å and becomes closer to the amine group nitrogen (1.27 Å). The phenyl ring proton is transferred to the head (amine group) via a 62.1 kcal/mol energy barrier (**TS-H**), (See SI, Table S4). As seen in Figure 5, isomerization of the p-PDA free-radical is not straightforward from the thermodynamic viewpoint, which is aligned with experimental findings rationalizing the favorable head-to-head polymerization.

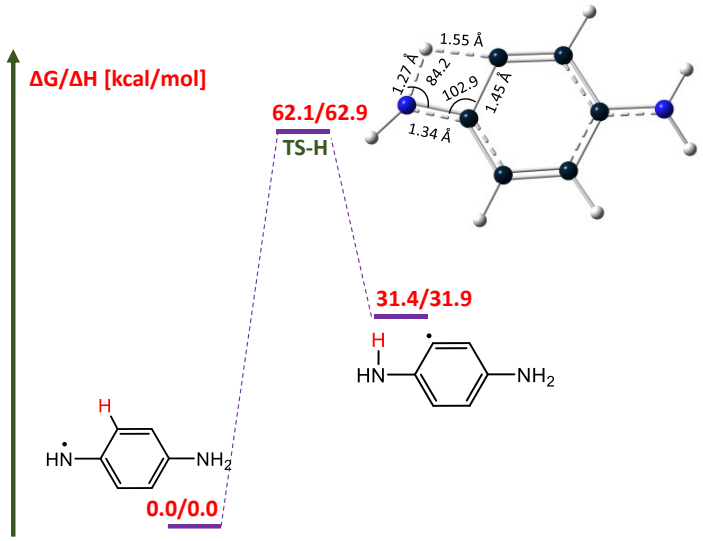

Figure 5. Reaction profile for the p-PDA free-radical internal proton migration (rearrangement: $\dot{N}H - C_6H_4 - NH_2 \overset{\sim H}{\longrightarrow} NH_2 - \dot{C}_6H_3 - NH_2$).

Based on the possible polymerization pathways (SFT, PA, and PP), we proposed the PP route as the best RP because of the shallow energy barriers. Therefore, the following mechanistic cycle was designed for the p-PDA polymerization reaction related to the PP route (Scheme 2).

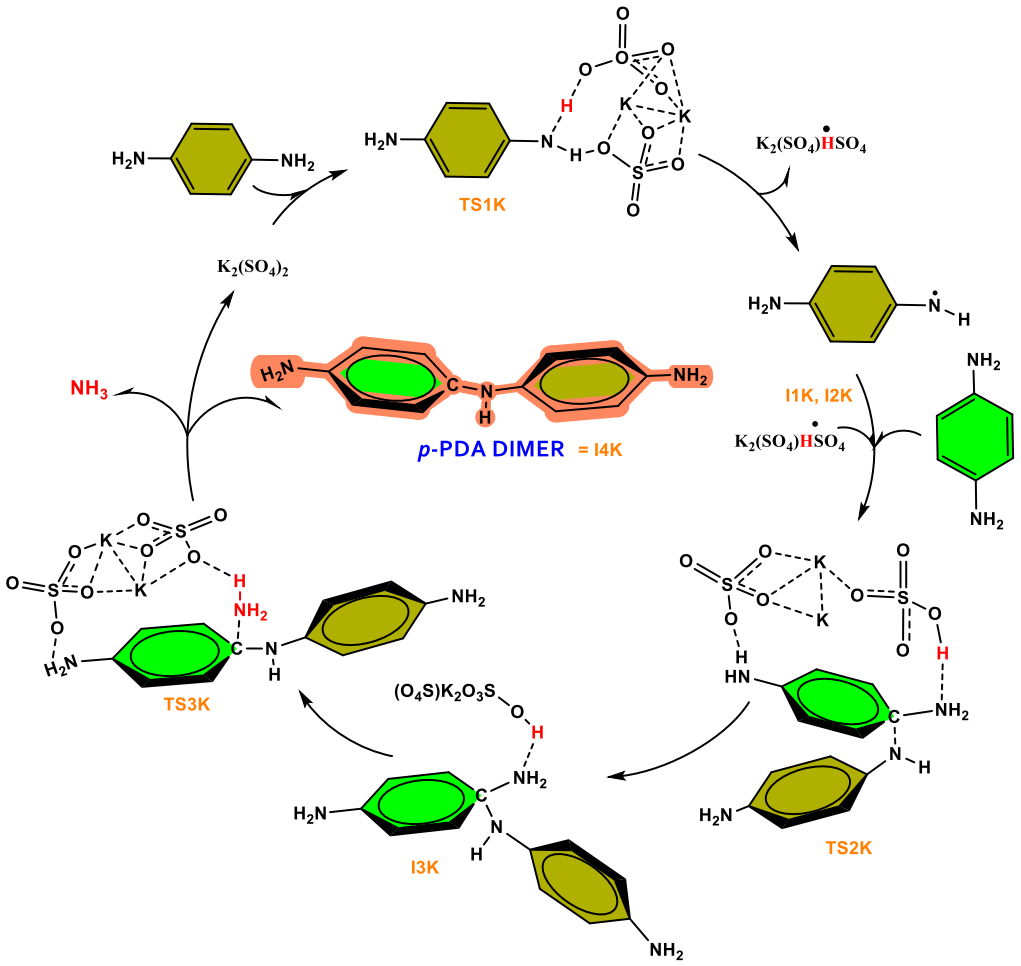

Scheme 2. Calculated mechanistic cycle of the p-PDA polymerization reaction up to the dimer (**I4K**) level.

Conclusions

Uncovering the mechanism that results in the formation of the p-PDA free-radical dimer (**DIMER-K**) is important to understand the p-PDA polymerization because poly-p-PDA and its modifications have extensive applications in electronic devices. The works focused on the frequently utilized polymerization oxidant/initiator potassium persulfate (PP) role in p-PDA dimerization. The polymerization mechanism

was displayed based on the replicated free-radical formation (monomer) → dimerization → ammonia extrusion → free-radical formation (dimer) steps. Since aqueous media was used experimentally, PP dissociation was considered, and the entire cycle was calculated trice: sulfate free-radical (SFR), persulfate anion (PA), and potassium persulfate (PP) cluster mediated routes. The PP route was studied in detail because of the lowest formation Gibbs energies of TSs and intermediates. The barrierless conversion of p-PDA to free-radical (**I1K**) promotes dimerization (**TS2K**) through the 11.6 kcal/mol energy barrier.

Further ammonia extrusion step leads to dimer formation (**TS3K**) via 6.7 kcal/mol energy. Then, the produced dimer (**I4K**) was calculated to convert to the free-radical dimer (**DIMER-K**) without an energy barrier. The PP cluster effects were scrutinized based on the binding via noncovalent interaction and eventually stabilizing p-PDA for facile free-radical conversion and dimerization.

Conflicts of interest

There are no conflicts to declare

Acknowledgments

Y.A. acknowledges the SOCAR Science Foundation, S/N 12LR-AMEA (05/01/2022). J.A. thanks The National Science Foundation, grant CHE 1560881, for support. All authors thank the Center for Computational Research (CCR) at the University at Buffalo for providing computational resources.

Data Availability Statement

The data that supports the findings of this study are available in the supplementary material of this article

References

1. Yang, W.; Zhou, H.; Huang, Z.; Li, H.; Fu, C.; Chen, L.; Li, M.; Liu, S.; Kuang, Y. Electrochimica Acta 2017, 245, 41-50.
2. Sousa, M. S. P.; de Sá, A. C.; de Oliveira, J. P. J.; da Silva, M. J.; Santos, R. J.; Paim, L. L. ECS Journal of Solid State Science and Technology 2020, 9(4), 041006.
3. Yang, C.; Zhang, M.; Dong, W.; Cui, G.; Ren, Z.; Wang, W. PLOS ONE 2017, 12(3), e0174104.
4. Riaz, U.; Jadoun, S.; Kumar, P.; Kumar, R.; Yadav, N. RSC Advances 2018, 8(65), 37165-37175.
5. Zhao, G.; Zhao, H.; Shi, L.; Cheng, B.; Xu, X.; Zhuang, X. Separation and Purification Technology 2021, 274, 119054.
6. Min, Y.-L.; Wang, T.; Zhang, Y.-G.; Chen, Y.-C. Journal of Materials Chemistry 2011, 21(18), 6683-6689.
7. Khokhar, D.; Jadoun, S.; Arif, R.; Jabin, S. Materials Research Innovations 2022, 26(1), 25-35.

8. Adachi, C.; Tsutsui, T.; Saito, S. Applied Physics Letters 1989, 55(15), 1489-1491.
9. Tian, J.; Li, H.; Luo, Y.; Wang, L.; Zhang, Y.; Sun, X. Langmuir 2011, 27(3), 874-877.
10. Jadoun, S.; Riaz, U.; Yáñez, J.; Pal Singh Chauhan, N. European Polymer Journal 2021, 156, 110600.
11. Sivakkumar, S. R.; Saraswathi, R. Journal of Applied Electrochemistry 2004, 34(11), 1147-1152.
12. Han, J.; Liu, Y.; Li, L.; Guo, R. Langmuir 2009, 25(18), 11054-11060.
13. Coote, M. L.; Krenske, E. H.; Izgorodina, E. I. Macromolecular Rapid Communications 2006, 27(7), 473-497.
14. Yildiko, Ü.; Ata, A. C.; Cakmak, İ. SN Applied Sciences 2020, 2(10), 1691.
15. Mavroudakis, E.; Cuccato, D.; Moscatelli, D. In Computational Quantum Chemistry; Soroush, M., Ed.; Elsevier, 2019, p 47-98.
16. McCormick, T. M.; Bridges, C. R.; Carrera, E. I.; DiCarmine, P. M.; Gibson, G. L.; Hollinger, J.; Kozycz, L. M.; Seferos, D. S. Macromolecules 2013, 46(10), 3879-3886.
17. Nifant'ev, I.; Vinogradov, A.; Vinogradov, A.; Ivchenko, P. Polymers 2020, 12(4).
18. Tardy, A.; Gil, N.; Plummer, C. M.; Zhu, C.; Harrisson, S.; Siri, D.; Nicolas, J.; Gigmes, D.; Guillaneuf, Y.; Lefay, C. Polymer Chemistry 2020, 11(45), 7159-7169.
19. Zhao, X.; Huang, W.; Lin, S.; Chen, X.; Guo, X.; Zou, D.; Ye, G. ACS Omega 2021, 6(24), 15608-15616.
20. Liang, Q.; Chang, X.; Su, Y.-q.; Mugo, S. M.; Zhang, Q. Angewandte Chemie International Edition 2021, 60(33), 18014-18021.
21. Lakard, B.; Herlem, G.; Lakard, S.; Fahys, B. Journal of Molecular Structure: THEOCHEM 2003, 638(1), 177-187.
22. Ullah, H.; Shah, A.-u.-H. A.; Ayub, K.; Bilal, S. The Journal of Physical Chemistry C 2013, 117(8), 4069-4078.
23. Cataldo, F. European Polymer Journal 1996, 32(1), 43-50.
24. Huang, M.-R.; Li, X.-G.; Yang, Y. Polymer Degradation and Stability 2000, 71(1), 31-38.
25. Durgaryan, A. A.; Arakelyan, R. A.; Durgaryan, N. A. Russian Journal of General Chemistry 2014, 84(6), 1095-1100.
26. Zhang, J.; Zhang, X.; Zheng, Y. Progress in Organic Coatings 2021, 158, 106330.
27. Frisch, M. J.; Trucks, G. W.; Schlegel, H. B.; Scuseria, G. E.; Robb, M. A.; Cheeseman, J. R.; Scalmani, G.; Barone, V.; Mennucci, B.; Petersson, G. A.; Nakatsuji, H.; Caricato, M.; Li, X.; Hratchian, H. P.; Izmaylov, A. F.; Bloino, J.; Zheng, G.; Sonnenberg, J. L.; Hada, M.; Ehara, M.; Toyota, K.; Fukuda, R.; Hasegawa, J.; Ishida, M.; Nakajima, T.; Honda, Y.; Kitao, O.; Nakai, H.; Vreven, T.; Montgomery Jr., J. A.; Peralta, J. E.; Ogliaro, F.; Bearpark, M. J.; Heyd, J.; Brothers, E. N.; Kudin, K. N.; Staroverov, V. N.; Kobayashi, R.; Normand, J.; Raghavachari, K.; Rendell, A. P.; Burant, J. C.; Iyengar, S. S.; Tomasi, J.; Cossi, M.; Rega, N.; Millam, N. J.; Klene, M.; Knox, J. E.; Cross, J. B.; Bakken, V.; Adamo, C.; Jaramillo, J.; Gomperts, R.; Stratmann, R. E.; Yazyev, O.; Austin, A. J.; Cammi, R.; Pomelli, C.; Ochterski, J. W.; Martin, R. L.; Morokuma, K.; Zakrzewski, V. G.; Voth, G. A.; Salvador, P.; Dannenberg, J. J.; Dapprich, S.; Daniels, A. D.; Farkas, Ö.; Foresman, J. B.; Ortiz, J. V.; Cioslowski, J.; Fox, D. J.; Gaussian 09, Revision D.01, Gaussian, Inc.: Wallingford, CT, USA, 2009.
28. Becke, A. D. Physical Review A 1988, 38(6), 3098-3100.
29. Lee, C.; Yang, W.; Parr, R. G. Physical Review B 1988, 37(2), 785-789.
30. Grimme, S.; Antony, J.; Ehrlich, S.; Krieg, H. The Journal of Chemical Physics 2010, 132(15), 154104.
31. Hehre, W. J.; Ditchfield, R.; Pople, J. A. The Journal of Chemical Physics 1972, 56(5), 2257-2261.
32. Chagovets, V. V.; Kosevich, M. V.; Stepanian, S. G.; Boryak, O. A.; Shelkovsky, V. S.; Orlov, V. V.; Leontiev, V. S.; Pokrovskiy, V. A.; Adamowicz, L.; Karachevtsev, V. A. The Journal of Physical Chemistry C 2012, 116(38), 20579-20590.

33. Li, X.-G.; Huang, M.-R.; Chen, R.-F.; Jin, Y.; Yang, Y.-L. Journal of Applied Polymer Science 2001, 81(13), 3107-3116.